J. Sound Vib. (1965) **2** (4), 435–461

POSSIBLE EXPLOITATION OF NON-LINEAR ACOUSTICS IN UNDERWATER TRANSMITTING APPLICATIONS

H. O. BERKTAY

Department of Electronic and Electrical Engineering, University of Birmingham, Edgbaston, Birmingham 15, England

(*Received 13 April 1965*)

Westervelt's approach to the calculation of non-linear effects in acoustic propagation is extended to the cases where the primary beams are spreading cylindrically or spherically. The results obtained are used to evaluate some possible applications in underwater acoustic transmission.

1. INTRODUCTION

That the propagation of acoustic waves is inherently of a non-linear nature has been known for a long time. Rayleigh (1) discusses in detail the approach of various workers of his time to the analysis of finite amplitude sound waves. A more up-to-date bibliography has been compiled by Kuljis (to be published).

Considerations pertaining to the scattering of sound waves also date back to Rayleigh's era.

Rayleigh considered the scattering of sound waves from regions in which both density and compressibility were assumed to be different from the values obtaining in the rest of the medium. He treated the scattered waves as small quantities so that they could be assumed to be propagated linearly.

Rayleigh's treatment can be extended to cover the case where the variation of density and compressibility in a given region of the medium is caused by a second sound wave, thus leading to a study of scattering due to interaction between sound waves.

More recently, Westervelt (2) extended Lighthill's work (3) on energy converted into sound waves from turbulence in fluids, and calculated the equivalent source density function which could be used in calculating (on a quasi-linear basis) the scattered field due to interaction of sound waves.

In the present paper an attempt is made to evaluate possible applications of acoustic non-linearities, using the quasi-linear approach of Westervelt. The basic concept of "Huygens wavelets" being created at all points in the common volume due to the interaction of sound waves appears to be essentially valid. The fact of their independent existence outside the common volume would appear to have been proven by experimental results so far available (4, 5). Further experiments are planned to establish the validity of this approach.

1.1. WESTERVELT'S APPROACH TO THE CALCULATION OF EFFECTS DUE TO ACOUSTIC NON-LINEARITIES

Westervelt considered primary waves interacting within a given volume and calculated the scattered pressure field due to the non-linearities within a small portion of this common volume in the medium. He ascribed this effect to volume distributed sources, of

volume density q, which were assumed to be created by the non-linear interaction of the primary waves, and considered effects due to the virtual sources contained in a small element of the common volume, the dimensions of which were taken to be infinitesimal. If Huygens wavelets are assumed to emanate from each such element, then the total scattered field at a point in the medium can be calculated by integrating the field due to all such wavelets. The source strength associated with each wavelet is $q\,dv$ where dv is the elemental volume and q, the source density, is a function of the position of the particular element within the volume of interaction of the primary waves.

The expression for the source-density obtained by Westervelt is

$$q = \frac{1}{\rho_0^2 c_0^4}\frac{\partial}{\partial t}(p_i^2)\left[1+\frac{\rho_0}{2c_0^2}\left(\frac{d^2p}{d\rho^2}\right)_{\rho=\rho_0}\right]. \tag{1.1}$$

A derivation of this expression by using small perturbation techniques has been carried out by Smith (6). A list of definitions of symbols is given in Appendix 5.

As an example, Westervelt (7) considered the special case of the interaction between two coincident collimated plane waves of different frequencies. In order to illustrate his approach, which will be used throughout the present paper, this case is studied in detail in Appendix 1. Westervelt pointed out that in fact, in this manner, an end-fire array of virtual acoustic sources could be produced.

This particular case was later studied experimentally by Bellin and Beyer (4) and, more recently, in the Department of Electronic and Electrical Engineering in the University of Birmingham (5). These experiments are discussed in section 2 of this paper.

1.2. WESTERVELT'S SOURCE DENSITY FUNCTION

The second term inside the square brackets in the expression for the source density function given in equation (1.1) depends upon the relationship between pressure and density in the acoustic medium. Assuming the process to be adiabatic, this term can be evaluated for gaseous media from the abiabatic equation of state

$$P\rho^{-\gamma} = P_0\rho_0^{-\gamma}$$

where γ is the ratio of the specific heats. Then,

$$\left(\frac{d^2p}{d\rho^2}\right)_{\rho=\rho_0} = \frac{\gamma(\gamma-1)P_0}{\rho_0^2},$$

$$= (\gamma-1)c_0^2/\rho_0$$

as $c_0^2 = \gamma P_0/\rho_0$. Therefore, the expression in the square brackets becomes $1+(\gamma-1)/2$.

Beyer (8) evaluated the parameter $(\rho_0/c_0^2)(\partial^2 p/\partial\rho^2)_{\rho=\rho_0}$ for water for an isentropic process, using the experimental results of other workers for variation of velocity of sound with pressure. His results indicate that the expression in square brackets in equation (1.1) has a value which varies between 3·1 when the water is at a temperature of 0° C, and 3·5 when the temperature is 20° C.

Whatever the value of this term for the medium being considered, it causes the expression in the source density function $(\partial/\partial t)(p_i^2)/(\rho_0^2 c_0^4)$, to be multiplied by a number larger than unity. In the rest of this paper this factor will be assumed to be unity in order to shorten the formulae; its appropriate value can be introduced into the results in the form of a simple multiplier.

A statement of the quasi-linear approach

Inherent in Westervelt's treatment of the problem of the scattering of sound waves due to non-linearities in acoustic propagation is the assumption that the second-order

effects produced by the interaction of acoustic waves are propagated in a linear fashion; in other words, that as they are second-order quantities themselves, distortion suffered by them in propagating in a non-linear manner will be negligible. This approximation is used throughout the present paper.

The method followed in calculating the effects due to the virtual sources is illustrated in greater detail in Appendix 1. Briefly, this consists of the calculation of the effects (velocity potential or differential pressure) at a point in the far field arising from a point source within the common volume, the source strength being the product of the source density and the elemental volume $\delta v = \delta x \delta y \delta z$. The distance of a point in the far field from the common volume is assumed to be large compared with the dimensions of the latter. The overall value of the scattered pressure at the point in the far field is then found by summing up all the similar effects, observed at the same point in the far field, due to all possible sources within the common volume.

2. END-FIRE ARRAYS OF VIRTUAL ACOUSTIC SOURCES

2.1. PRELIMINARY EXPERIMENTS

Westervelt (7) and Bellin and Beyer (4) considered an end-fire array of virtual sources formed by the interaction of two coincident plane waves of different frequencies. This case is analysed in detail in Appendix 1. One can visualize however, the difference frequency waves created by the interaction of two coincident plane waves adding up in phase only along the direction of propagation of the primary waves, thus producing an end-fire effect.

To produce two collimated and coincident planar waves experimentally, Bellin and Beyer transmitted the two primary waves from the same transducer, a circular 13·5 Mc/s quartz transducer, 1 in. in diameter. As the absorption coefficient of water at such high frequencies is very high, interaction between the two waves is effectively confined to the near field of the transducer.

In the near field of a piston the propagating waves are known to be (9) well-collimated and to approximate to plane waves.

They measured the beam width produced by the virtual end-fire array at difference frequencies ranging between 1 Mc/s and 2 Mc/s.

The treatment of the virtual end-fire array in references (4) and (7) is based on the implicit assumption that the column of primary waves has a cross-sectional area the dimensions of which are negligible compared with the wavelength at the difference frequency. However, in the experiments reported in reference (4), the wavelengths at the difference frequency ranged between 0·75 mm (at 2 Mc/s) and 1·5 mm (at 1 Mc/s), while the diameter of the primary column was about 1 in. (25·4 mm).

The results obtained by Bellin and Beyer (4) showed that the differential pressure at a point along the axis of the transducer and at the difference frequency was about 3 dB below that predicted on the basis of Westervelt's theory, and that the beam width of the end-fire effect, measured between the half-pressure points on a plane including the axis, showed the expected form of dependence on the frequency, but that the actual values of the beam width were smaller than those predicted by them.

The result obtained by Westervelt for the differential pressure at the difference frequency at a point (R, θ) in the far field (measured from the centre of the transducer and from the normal axis of the transducer, respectively) can be given as

$$p(R,\theta) = \frac{P_1 P_2 \Omega^2 S}{4\pi\rho_0 c_0^4 R} \exp(-\alpha R) \frac{\cos(\Omega t - KR - \beta)}{\{A^2 + [2K\sin^2(\theta/2)]^2\}^{1/2}}, \tag{2.1}$$

where P_1 and P_2 are the pressure amplitudes of the primary waves, referred back to the transducer surface. The other symbols are:

S cross-sectional area of the primary beams;
$A = \alpha_1+\alpha_2-\alpha\cos\theta$;
$\fallingdotseq \alpha_1+\alpha_2-\alpha$, provided $\theta \ll 1$;
α_1, α_2 absorption coefficients of the primary sound waves;
α that for the difference frequency wave;
$\tan\beta = A/[2K\sin^2(\theta/2)]$.

For a given value of R, the pressure amplitude becomes maximum when $\theta = 0$; i.e., when the observer is along the axis of the transducer.

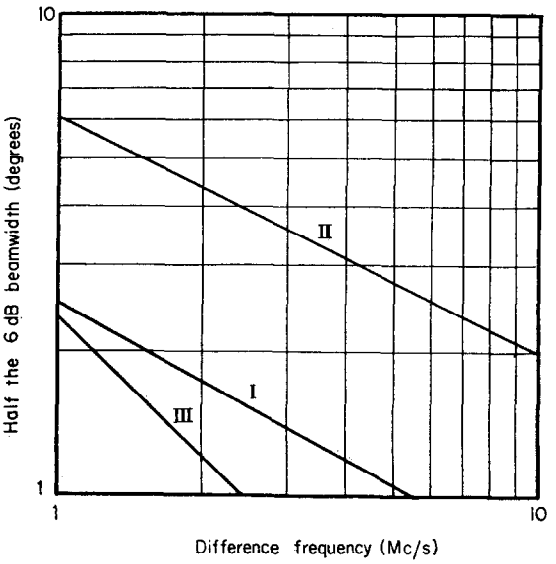

Figure 1. Bellin and Beyer's experiment. Curve I, experimental results; curve II, results predicted from equations (2); curve III, predicted for radiation from a circular aperture of 1 in. diameter.

Thus, the pressure amplitude is 3 dB below maximum when $2K\sin^2(\theta/2) = A$, that is, when

$$\sin(\theta/2) = \pm\sqrt{(A/2K)}. \tag{2.2}$$

Bellin and Beyer (4) consider the values of θ for which the pressure amplitude is reduced to 1/2 its maximum value, i.e. the -6 dB points. This would occur when

$$2K\sin^2(\theta/2) = A\sqrt{3}.$$

When $A/(2K) \ll 1$, equation (2.2) gives the 3 dB beam width as

$$2\theta_d = 4\sqrt{A/(2K)}. \tag{2.3}$$

If, however, S is large compared with λ^2, λ being the wavelength at the difference frequency, equation (2.1) includes a factor (aperture effect) which in two-dimensional geometry would be of the form $(\sin x)/x$ or of $2J_1(x)/x$ depending upon whether the beams are of rectangular or circular cross-section (see Appendix 1).

Figure 1 has been prepared for the conditions pertaining to the experiments of Bellin and Beyer. Curve I represents the line fitted to the experimentally obtained points for

half the 6 dB beam width; II is the curve predicted from equation (2.1), while III is that for a circular piston of 1 in. diameter radiating at the difference frequency.

It can be seen that although the experimental results show the predicted law of dependence upon the difference frequency, they are about 0·4 of the expected values.

The experiment was repeated in the Department of Electronic and Electrical Engineering of the University of Birmingham (5), using a square 3 Mc/s transducer 9 cm^2 in area, the 3 dB beam width being measured at various difference frequencies. The results for 3 dB beam widths in a horizontal plane through the axis are shown in Figure 2. Also shown on the same figure are the curves computed from equation (2.1) (curve II) and from equation (2.1) modified by the aperture factor of the form $(\sin x)/x$ (curve I). Curve III of Figure 2 is calculated for a square piston radiating at the difference frequency.

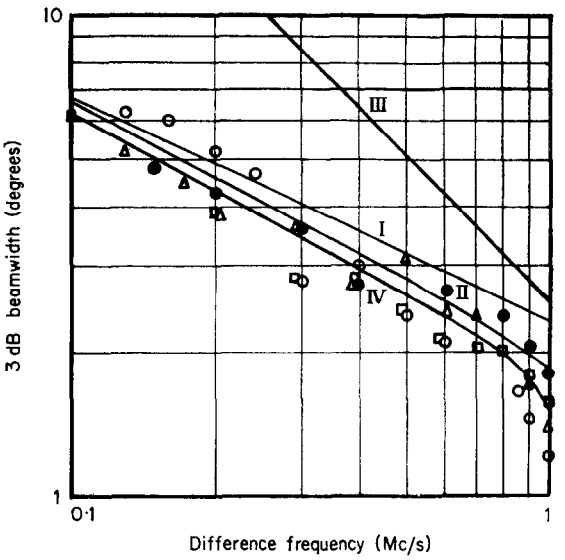

Figure 2. Experiment carried out at the University of Birmingham. Curve I, predicted from equation (3); curve II, as for curve I, but allowing for the aperture factor as well; curve III, predicted for radiation from a square aperture of an area 9 cm^2; curve IV, the average of various runs. (○, ●, △, □). Experimental results obtained at various runs.

The experimental results shown in Figure 2 are in good agreement with the theory. It has not been possible, to date, to measure the absolute values of the differential pressure at the difference frequency. However, it is expected that the instrumentation problems necessary for such measurements will be solved shortly.

2.2. POSSIBLE APPLICATION TO THE PRODUCTION OF LOW FREQUENCY SOUND WAVES

From equation (I.9) of Appendix 1 the amplitude of the differential pressure at the difference frequency along the axis of symmetry of two superimposed primary waves can be given in the form

$$P = \frac{\sqrt{W_1 W_2}\,\Omega^2}{2\pi c_0^3 RA} \exp(-\alpha R). \tag{2.4}$$

It is further pointed out in Appendices 1, 2 and 3 that the pressure amplitude at a point along the axis of symmetry is largely independent of whether the primary waves are collimated plane waves, or cylindrically or spherically spreading waves, provided the

3 dB beam width of the beam formed by the two primary waves is not much greater than $2\theta_d$, which has the value given in equation (2.3) and is the 3 dB beam width of the end-fire array of small cross-sectional area studied by Westervelt. The absorption coefficients of fresh water and sea water at 5° C are shown in Figure 3 and the values of θ_d for various values of primary and difference frequencies, and for propagation in both fresh water and sea water are given in Figure 4(a) and (b).

Assuming, for the moment, that the acoustic powers transmitted in the two primary waves are equal (i.e., that $W_1 = W_2 = W/2$), one finds from equation (2.4) that

$$P \fallingdotseq \frac{\pi W(f_1-f_2)^2}{c_0^3 RA}\exp(-\alpha R). \tag{2.5}$$

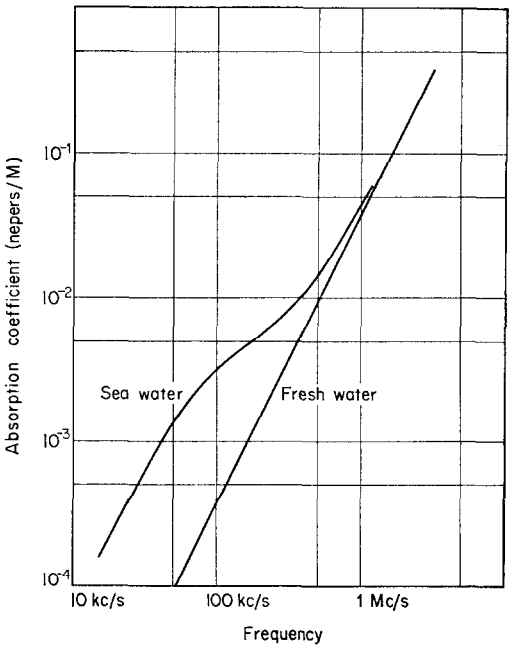

Figure 3. Absorption coefficient of water at 5° C.

It is worth noting that if power W_E is transmitted from an omnidirectional source, at frequency (f_1-f_2), the pressure amplitude at a distance R would be

$$P_E = \left(\frac{\rho_0 c_0 W_E}{2\pi}\right)^{1/2}\frac{1}{R}\exp(-\alpha R). \tag{2.6}$$

Comparing (2.5) and (2.6), if $W = W_E$, gives

$$P/P_E = \left(\frac{\pi^3 W}{2\rho_0 c_0}\right)^{1/2}\frac{(f_1-f_2)^2}{Ac_0^3}. \tag{2.7}$$

For water, putting $\rho_0 = 10^3$ kg/m^3 and $c_0 = 1500$ msec, this becomes

$$P/P_E = \frac{W^{1/2}(f_1-f_2)^2}{A}\times 10^{-13}. \tag{2.8}$$

The following example illustrates the situation. Let $\frac{1}{2}(f_1+f_2) = 20$ kc/s. Then, in sea water, $A \fallingdotseq 6\times 10^{-4}$ nepers/metre. For $(f_1-f_2) = 1$ kc/s, then

$$P/P_E = 1{\cdot}6\times 10^{-4}\sqrt{W}.$$

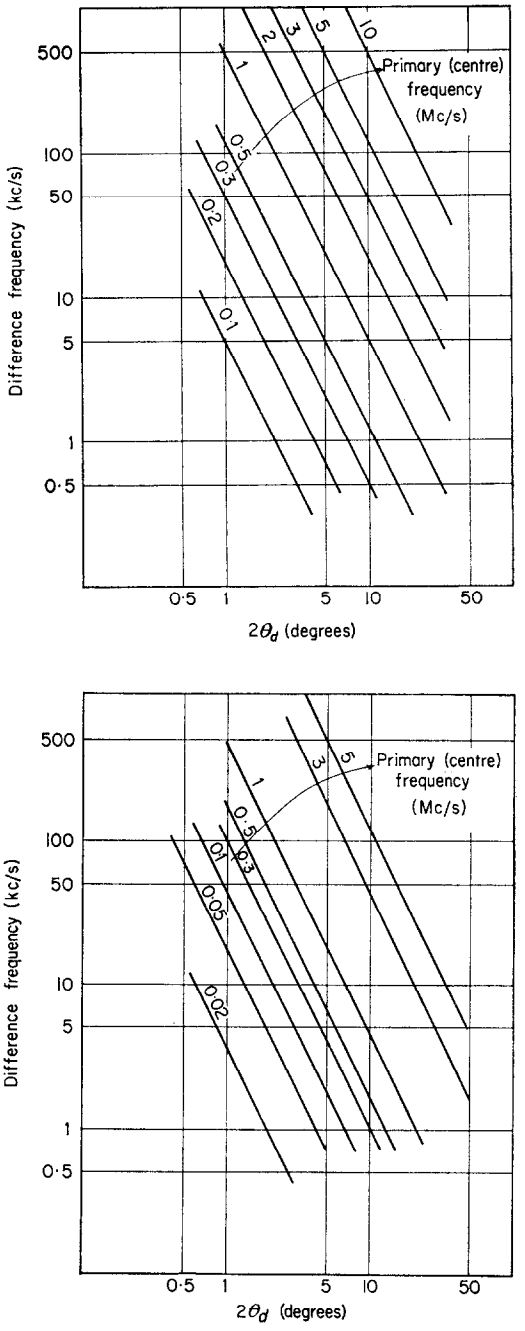

Figure 4(a), (b). Beam width at difference frequency for various values of primary frequencies, calculated from $2\theta_d = 4\,(A/2K)^{1/2}$; (a), fresh water at 5° C, (b), sea water at 5° C.

Thus, the conversion process is inefficient for practicable values of transmitted power. For example, if $W = 100$ kW, then

$$P/P_E = 5 \times 10^{-2},$$

or $P = P_E$ if $W_E = W/400$.

Thus, for purposes of obtaining a desired pressure magnitude at a given radius from the source, the end-fire array principle is grossly inefficient.

However, when the obtaining of a sharp beam *or* very narrow pulse (i.e., lower effective Q for the transducer) is of importance, then it should be borne in mind that the estimated 3 dB beam width in the above example is of the order of 2° and, on the assumption that $Q = 10$ for the 20 kc/s transducer, a pulse of 1 msec duration at a virtual carrier frequency of 1 kc/s becomes feasible.

Launching of large powers of coherent acoustic waves into water at low frequencies is a difficult process. The difficulties arise from the need for large piston area and from the need to work with low acoustic intensities if cavitation is to be avoided.

In the example considered above, the wavelengths at the primary frequencies are of the order of 7·5 cm whereas that at the difference frequency of 1 kc/s is 1·5 m. Thus, a transducer the dimensions of which are large compared with the wavelength can be constructed with comparative ease at 20 kc/s, rather than at 1 kc/s.

Further, as pulses of duration of the order of 1 msec become possible, acoustic waves of much higher peak intensities may be launched without cavitation. This can be seen from Hueter and Bolt (11), Figure 6.19, for example. When pulse duration is reduced to about 1 msec the cavitation threshold increases very rapidly.

Thus, it can be concluded that although the power conversion process is very inefficient, the use of the non-linear interaction between two waves to generate a low frequency sound wave has some advantages over the direct launching of such a wave in water.

3. A LOW FREQUENCY SECTOR-SCANNING ARRAY

The principles of electronic scanning arrays and their application to sonar systems are well known. However, to obtain a narrow scanning beam at low frequencies, the transducer size required increases prohibitively. For example, to obtain a 1° fan beam at a frequency of 7 kc/s one would require a transducer about 12 m long. The mounting and stabilization of such a transducer would present problems. To reduce the transducer size, the frequency normally is increased to hundreds of kc/s, which results in a reduction in the system range because of the increased absorption of the sound energy at these higher frequencies.

As pointed out previously, the pressure amplitude along the axis of symmetry of a virtual end-fire array formed by the non-linear interaction of two primary waves is expected to be independent of the shape of the primary beams, provided the beam width of the primary waves is small. This result should permit the use of cylindrically or spherically spreading primary waves to form virtual end-fire type arrays, which, in turn, would lead to the possibility of obtaining a sector-scanning transmitting beam, the physical array having dimensions corresponding to the wavelength at the primary frequencies.

Example (i): *a 7 kc/s beam in sea water*

For $(f_1+f_2)/2 = 100$ kc/s and $(f_1-f_2) = 7$ kc/s, $\theta_d \doteqdot 1°$ in sea-water, giving an expected 3 dB beam width of about 2°. As the spreading angle of the primary beam must be of the order of $2\theta_d$ (see Appendices 2 and 3), the 100 kc/s transducer must produce a beam of about 2° along both axes, which implies, say, a transducer of about 45×45 cm. It is worth noting that this dimension is only about 2 wavelengths at 7 kc/s.

Using equation (2.5) and neglecting absorption at 7 kc/s, gives the rms value of the differential pressure along the axis of the beam as $\bar{P} = 53\ W/R\ \mu$bar, where W is the total acoustic power in the primary beams, in watts, and R is in metres. For these condi-

tions, from equation (2.7), $P/P_E = 7{\cdot}8 \times 10^{-3}\sqrt{W}$. Thus, for $W = 16$ kW, $P = P_E$. For a transducer area of about 1600 cm^2 this gives an intensity of about 10 watts/cm^2.

As transmission is now at about 100 kc/s and as shorter pulses may thus be transmitted, the cavitation threshold will be higher and peak power densities of the order of 10 watts/cm^2 can be transmitted. This will clearly depend upon the pulse length utilized [see Hueter and Bolt (11), for example]. In this case, peak powers greater than 20 kW could be transmitted quite easily by using a transducer of about 0·5 m^2 transmitting area, without reaching the threshold of cavitation.

Example (ii): *a scale model.*

Another example provides information relevant to making a scale model to try in fresh water. When $(f_1+f_2)/2 = 600$ kc/s and $(f_1-f_2) = 7$ kc/s, then in fresh water $2\theta_d = 5°$. Hence, the primary waves must be confined within a beam of about 5° in width.

At 600 kc/s, this means a minimum transducer size of about 3 cm × 3 cm (as $\lambda = 0{\cdot}25$ cm). Calculations indicate that the pressure at 1 m per watt of transmitted acoustic power, should be of the order of 10 μbar (rms). In other words, for a total transmitted peak power of about 100 watts, it should be possible to obtain a detectable signal at a distance of about 100 m.

If scanning over a 10° sector is required, the individual transducers must not be more than about 5λ in width along the axis of scan; i.e., of the order of 1 cm.

If a larger array is made and higher peak powers utilized then appreciable signals will be obtained.

It is hoped that experiments will be carried out shortly with a view to demonstrating the feasibility of such a project.

4. PULSE PRODUCED BY THE SELF-DEMODULATION OF A PULSED CARRIER

When an acoustic wave in the form of a pulsed carrier is propagating in a homogeneous fluid, the so-called radiation pressure measured at a fixed point is known to follow the envelope of the wave. In fact, this phenomenon has been used to measure the intensity of acoustic waves (12). However, the possibility of this effect being able to propagate independently of the primary wave giving rise to it has not been considered previously.

Because of the non-linearity of acoustic propagation, the primary wave will interact with itself. If one assumes that the pulsed carrier type acoustic wave is collimated and plane, and is travelling along the x-direction, the primary differential pressure at a point x at time t can be represented in the form

$$p_i(t,x) = P_1 \exp(-\alpha_1 x) f\left(t-\frac{x}{c_0}\right) \cos(\omega_1 t - k_1 x) \tag{4.1}$$

where $f(t)$ represents the envelope function, in the frequency spectrum of which the highest Fourier component has a very much lower frequency than the carrier. This condition permits the use of α_1 as the absorption coefficient for this band-limited signal.

In equation (1.1), the effective source density is shown to depend upon the partial time derivative of p_i^2. From (4.1) however,

$$p_i^2(t,x) = (1/2) P_1^2 \exp(-2\alpha_1 x) f^2\left(t-\frac{x}{c_0}\right)[1+\cos(2\omega_1 t - 2k_1 x)]. \tag{4.2}$$

Thus, two components are obtained in the expression for p_i^2 as a result of the self-interaction of the pulsed carrier wave; one of the components is a band-limited signal at twice

the carrier frequency, and the scattered waves due to this component will be attenuated relatively rapidly. The component of interest is that without the carrier term. As this term constitutes a compression only, it may be argued that it cannot propagate. However, any scattering due to this component will depend on an effective source function which is proportional to the partial time derivative of this component in the expression for p_i^2. Thus, the average value of the term is removed and positive and negative alternances are established for the effective source function. It is expected, therefore, that scattering will take place due to this component. To illustrate the point made, an example was worked out, assuming the envelope function, $f(t)$, to be Gaussian. The shape of the corresponding pressure pulse expected to be received at a point along the axis of symmetry is shown in Figure 5.

Detailed analysis of this phenomenon is carried out in Appendix 4. It is shown there that because of the end-fire array effect, most of the pulse energy can be concentrated within a small solid angle, forming a narrow pencil beam.

From equation (IV.25) of Appendix 4, the 3 dB beam width is expected to have an approximate value of

$$2\theta_1 = 4\sqrt{Ac_0/(5{\cdot}6n)} \tag{4.3}$$

for a Gaussian shaped envelope pulse of the form

$$f(t) = \exp(-n^2 t^2). \tag{4.4}$$

Further, the shape of the pulse received at a point at a distance R along the axis of symmetry is shown in equation (IV.9) to be related to the envelope pulse, $f(t)$, by

$$p(R,t) = \frac{P_1^2 S}{8\pi\rho_0 c_0^4 R\alpha_1}\frac{\partial^2}{\partial t^2}\left\{f^2\left(t-\frac{R}{c_0}\right)\right\},$$

where no restrictions are put on the form of $f(t)$ except that it has a maximum value of unity. Thus, denoting the peak transmitted power by W_0, one obtains

$$p(R,t) = \frac{W_0}{2\pi c_0^3 R\ (2\alpha_1)}\frac{\partial^2}{\partial t^2}\left\{f^2\left(t-\frac{R}{c_0}\right)\right\}. \tag{4.5}$$

For example, if $f(t)$ is as given in (4.4), then

$$\frac{\partial^2}{\partial t^2}\left\{f^2\left(t-\frac{R}{c_0}\right)\right\} = 4n^2\left[4n^2\left(t-\frac{R}{c_0}\right)^2-1\right]\exp\left[-2n^2\left(t-\frac{R}{c_0}\right)^2\right]. \tag{4.6}$$

The shape of the pressure pulse is indicated in Figure 5.

The time differentiation inherent in the scattering process results in the narrowing of the pulse and in the spreading of its energy over a wider frequency spectrum.

For example, the Fourier transform of $f(t)$ as given in (4.4) is

$$F(\omega) = \frac{\pi}{n}\exp[-\omega^2/(4n^2)],$$

giving for the Fourier transform of $\partial^2/\partial t^2\{f^2(t)\}$, the expression

$$-\frac{\omega^2\sqrt{(\pi/2)}}{n}\exp[-\omega^2/(8n^2)]. \tag{4.7}$$

The energy flow per unit area per pulse at a point along the axis at a distance R from the transducer, E, is calculated in Appendix 4 and the quantity $E_{eq} = 4\pi R^2 E$ [i.e., the energy per pulse which, if transmitted from an omnidirectional source would give the same energy intensity E, at the point $(R,0)$] is compared with E_0, the actual energy

transmitted per modulated pulse, the envelope of which is of the form given in equation (4.4). This ratio, which gives a measure of the gain of the system over an omnidirectional source, works out as [see equation (IV.31)]

$$E_{eq}/E_0 = \frac{E_0 \times 10^{-9}}{\alpha_1^2 t_m^5},$$

$$= \tfrac{1}{2}\sqrt{(\pi/2)}\frac{W_0}{\alpha_1^2 t_m^4} \times 10^{-12}, \tag{4.8}$$

where t_m is the duration (msec) of the transmitted pulse measured between its 1/e points, and is related to n by

$$t_m \times 10^{-3} = 2/n. \tag{4.9}$$

It is worth noting that the 1/e point of the spectrum of the transmitted pulse occurs for $f = 0{\cdot}64/t_m$ kc/s.

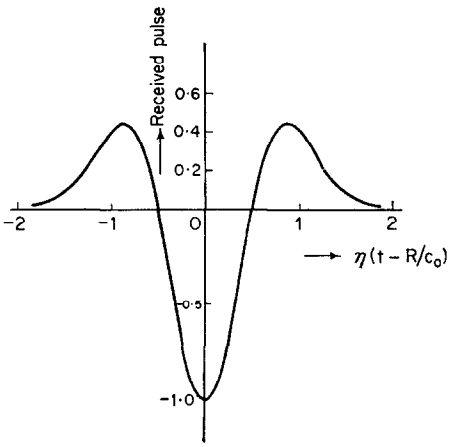

Figure 5. The shape of the received pulse when the transmitted carrier has a Gaussian envelope.

For a carrier frequency of 20 kc/s, in sea water, $\alpha_1 \doteqdot 3 \times 10^{-4}$ nepers/m. Then,

$$E_{eq}/E_0 = 0{\cdot}7 \times 10^{-5}(W_0/t_m^4).$$

Thus, even for a pulse of 1 msec duration, the energy intensity produced may be made of the same order as that which would be produced if the same amount of energy had been directly transmitted from an omnidirectional source.

In fact, $E_{eq}/E_0 = 1$ when $W_0/t_m^4 = 130{,}000$; i.e., for $t_m = 1$ msec, the peak acoustic power transmitted must be of the order of 130 kW.

The advantages of this system can be summarized as follows:

(1) the propagated energy is distributed over a wider frequency band in a manner which can be predetermined; this would lend itself to the use of signal processing techniques upon reception;

(2) the expected beam width of the transmission discussed in the example above is about 3°; this in itself might find rather limited application when reflections from layered media are being considered; however, it would be of use if smaller objects or discontinuities are to be charted;

(3) as the carrier frequency used is relatively high and the pulse duration is short, higher transmitted power densities may be utilized without cavitating the water.

So far, the primary wave has been considered to be plane. However, the calculations given in Appendices 2 and 3 indicate that, provided the primary beam is narrow, spherical or cylindrically spreading primary waves ought to give similar results.

5. DISCUSSION AND CONCLUSIONS

Strictly speaking, the quasi-linear approach used in studying the effects of non-linearities should be limited to relatively low power densities. When the power density is increased, it is possible that other effects, such as multiple scattering, will make the results estimated in the previous sections as regards possible applications of non-linearities grossly optimistic.

An advantage of the use of non-linear effects has been pointed out to be the possibility of forming long arrays of virtual sources.

A possible difficulty in the formation of a long virtual array in water might be thought to arise from turbulence. However, previous work on propagation phenomena suggests that turbulence as such may not be a serious problem. On the other hand, temperature differences within the region where the virtual array is formed might reduce the effective gain of this array. Serious deterioration of performance is not expected, however, if the isothermal surfaces are in the form of parallel layers, the layer size being at least comparable to the cross-section of the beams.

At low transmitted powers, the non-linear conversion process, which is basically one of second-order distortion, is very inefficient. This is the conclusion reached in section 2 where the obtaining of a very low frequency signal as the intermodulation product of two waves of frequencies of the order of 20 kc/s was considered.

A method which may be used to obtain a low frequency pressure pulse of a form which may be controlled by suitable shaping of the envelope which pulse modulates the carrier is discussed in Section 4. It is indicated that it may be possible to use this method to advantage if high peak powers may be transmitted.

Extension of Westervelt's work to cylindrically and spherically spreading waves indicates the possibility of producing a sector-scanning transmitting array, the dimensions of which would be determined by the wavelength at the primary frequencies, rather than that at the difference frequency. The example worked out in Section 3 indicates that acceptable effective signal levels may be obtained as well as a sharp beam at the relatively low frequency of 7 kc/s (i.e., at a wavelength of about 20 cm).

In spite of the inherent inefficiency of the power conversion process, some possible practical advantages can be foreseen for the use of acoustic non-linearities. In the applications considered in the present paper the advantages which can be obtained arise mainly from the use of high frequency primary waves to obtain highly directional acoustic energy at low frequencies.

The launching of acoustic waves is easier and more efficient at higher frequencies, as

(i) the bandwidth of the transducer is much greater than that obtainable at the low frequencies, thus permitting the use of much shorter pulses at a low frequency;

(ii) either high frequencies and/or short pulses are being transmitted, so that acoustic waves of much higher peak intensities may be launched without causing cavitation in the medium;

(iii) physical transducers of reasonable size can be used at the higher primary frequencies to concentrate the primary power within narrow beams and in this way long virtual arrays can be produced, the length of which in terms of the wavelengths at the difference frequency determines the directivity of the low frequency waves.

The use of non-linear acoustics may be viable in applications in which the advantages mentioned above offset the disadvantage of the inefficient conversion of power.

In addition to the applications so far considered, non-linear interaction can be used to provide a signal which is continuously variable in frequency for, say, calibration of hydrophones or of receivers, or possibly, for wide band sonar. This is made possible by the large transducer bandwidths available at the higher primary frequencies.

ACKNOWLEDGMENTS

The author gladly acknowledges numerous stimulating discussions with many colleagues, in particular with V. G. Welsby and B. K. Gazey. His thanks are also due to Professor D. G. Tucker for useful criticism of the manuscript during its preparation.

APPENDIX 1

END-FIRE ARRAY OF VIRTUAL SOURCES: AN EXTENSION OF WESTERVELT'S APPROACH

FORMULATION OF THE PROBLEM

In this Appendix an account is given of a detailed study of the effects due to the interaction between two collimated and coincident plane waves of different frequencies. The cross-section of the column is assumed to be rectangular.

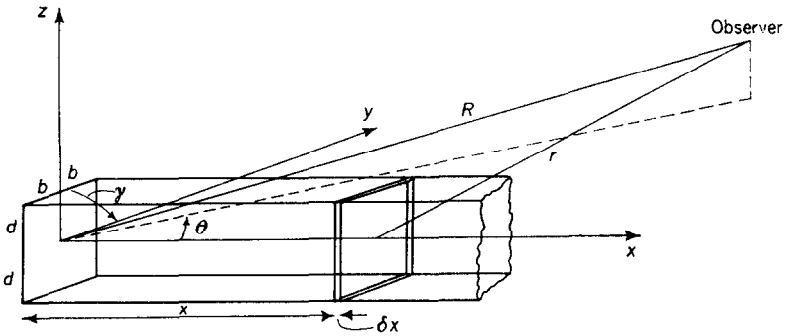

Figure 6. The geometry used. End-fire array formed by collimated planar primary waves.

The source density function can be evaluated using equation (1.1) of Section 1 if the pressure field due to the primary waves, p_i, is known. If an elemental volume $\delta x \delta y \delta z$, situated at a point (x,y,z) within the region common to the primary waves, contains an effective source of strength $q(t)\delta x \delta y \delta z$, then the scattered pressure field δp, due to this point source at a point of distance r from it is [see, e.g., pp. 217–218 of reference (13)]

$$\delta p(r,t) = -\frac{\rho_0}{4\pi r}\exp(-\alpha r)\,\delta x\,\delta y\,\delta z\,\frac{\partial}{\partial t}\left\{q\left(t-\frac{r}{c_0}\right)\right\}. \qquad (I.1)$$

Integration of this expression with respect to x, y and z, for all values within the boundaries of the common volume, gives the total pressure field at the point to which equation (I.1) refers. The geometry used is indicated in Figure 6. It is assumed that the two primary waves are launched from the same plane transducer and that the waves are both plane and well collimated. Then the total differential pressure at a point (x,y,z) due to the primary waves can be expressed as

$$p_i = P_1\exp(-\alpha_1 x)\cos(\omega_1 t - k_1 x) + P_2\exp(-\alpha_2 x)\cos(\omega_2 t - k_2 x), \qquad (I.2)$$

when $|y| \leqslant b$ and $|z| \leqslant d$, p_i being zero when y and/or z are (is) outside the limits specified above.

The source density function depends upon p_i^2; therefore it will have components at the frequencies $2\omega_1$, $2\omega_2$, $\omega_1 \pm \omega_2$. The effects due to the difference frequency component in the source function will be studied in the remainder of this Appendix.

The difference frequency term in the source function arises from the term

$$P_1 P_2 \exp(-\overline{\alpha_1+\alpha_2}\, x)\cos(\Omega t - Kx), \tag{I.3}$$

where $\Omega = \omega_1 - \omega_2$ and $K = k_1 - k_2$.

By substituting this for p_i^2 in the expression for the source function, the difference frequency component of the latter is obtained. This is

$$q = -\frac{\Omega}{\rho_0^2 c_0^4} P_1 P_2 \exp(\overline{\alpha_1+\alpha_2}\, x)\sin(\Omega t - Kx). \tag{I.4}$$

Thus, a cross-sectional wafer at x and of thickness δx includes a uniform distribution of co-phasal virtual sources. Hence, radiation from such a wafer is identical to that from a uniformly insonified aperture of the same shape and size. As the cross-section consists of a rectangle $2b \times 2d$, the radiated field at a point in the far field of the aperture is proportional to

$$(2d)(2b)\frac{\sin(dK\cos\gamma)}{(dK\cos\gamma)}\frac{\sin(bK\sin\gamma\sin\theta)}{(bK\sin\theta\sin\gamma)}. \tag{I.5}$$

The aperture effect, due to the finite cross-section of the volume-distributed virtual sources, having thus been isolated, the integration over x to obtain the over-all scattered pressure reduces to that obtaining in an end-fire array with exponential taper. This last is the case studied by Westervelt and by Bellin and Beyer.

If, for simplicity, the observer is restrained to move on the plane $z = 0$ in the far field (i.e., $r \gg x$, thus giving $R \fallingdotseq x\cos\theta + r$ when $\gamma = \pi/2$), then $\gamma = \pi/2$. The amplitude of the scattered pressure field can then be found by integration of equation (I.1), and is

$$P(R,\theta) = \frac{P_1 P_2 \Omega^2 (2b)(2d)}{4\pi\rho_0 c_0^4 R}\exp(-\alpha R)\frac{\sin(bK\sin\theta)}{(bK\sin\theta)}\frac{1}{[A^2+4K^2\sin^4(\theta/2)]^{1/2}} \tag{I.6}$$

AXIAL PRESSURE

If the observer is on the axis of symmetry of the transducer, $\theta = 0$. Then the amplitude of the differential pressure at the difference frequency is

$$P(R,0) = \frac{P_1 P_2 \Omega^2 S}{4\pi\rho_0 c_0^4 RA}\exp(-\alpha R), \tag{I.7}$$

where $S = 2b \times 2d$ is the cross-sectional area of the column.

As the primary waves are assumed to be plane and collimated, the acoustic powers in the waves at $x = 0$ are, respectively,

$$W_1 = SP_1^2/(2\rho_0 c_0) \tag{I.8}$$

and

$$W_2 = SP_2^2/(2\rho_0 c_0).$$

Substituting for P_1 and P_2 in equation (I.7), one obtains for the axial pressure amplitude

$$P(R,0) = \frac{\sqrt{(W_1 W_2)}\,\Omega^2}{2\pi c_0^3 RA}\exp(-\alpha R). \tag{I.9}$$

BEAM-WIDTH

From (I.6) and (I.7), a function $D(\theta)$ can be defined as

$$D(\theta) = P(R,\theta)/P(R,0) = \frac{\sin(bK\sin\theta)}{(bK\sin\theta)}\left\{1+\left[\frac{2K}{A}\sin^2(\theta/2)\right]^2\right\}^{-1/2}. \tag{I.10}$$

$D(\theta)$ gives the two-dimensional directivity pattern of the array of the virtual sources, and consists of two factors, one being that due to the finite aperture formed by the cross-section of the column and the other that due to the end-fire array with exponential taper.

If $bK \ll 1$, the aperture factor is unity. The 1/2 power points of the directivity pattern therefore occur when

$$\frac{2K}{A}\sin^2(\theta/2) = 1. \tag{I.11}$$

The value of θ satisfying this equation will be denoted by θ_d.

For propagation in water at the frequencies of general interest, $(A/2K) \ll 1$. Absorption coefficients for fresh water and for sea water are plotted in Figure 3 of Section 2, from the formulae given in reference (10).

Then from equation (I.9),

$$\sin(\theta_d/2) = \sqrt{(A/2K)} \ll 1,$$

and hence

$$(\theta_d/2) \doteq \sqrt{(A/2K)}. \tag{I.12}$$

Therefore, the 3 dB beam width of the end-fire array with small cross-sectional dimensions is given by

$$2\theta_d = 4\sqrt{(A/2K)}. \tag{I.13}$$

It is worth noting that the factor in the expression for $D(\theta)$ due to the end-fire effects does not have any maxima other than at $\theta = 0$ for $0 \leqslant \theta \leqslant 2\pi$, and is a minimum when $\sin(\theta/2) = 1$, that is, when $\theta = \pi$.

In a general case, the directivity pattern for the end-fire effects will be modified by an aperture factor, which in the case of a circular cross-section is of the form $2J_1(M)/M$. The effect of the aperture factor is to reduce the 3 dB beam width obtainable to values less than $2\theta_d$, θ_d being given by equation (I.11).

APPENDIX 2

END-FIRE ARRAY OF VIRTUAL SOURCES WHEN THE PRIMARY WAVES ARE SPREADING CYLINDRICALLY

The primary waves are assumed to consist of two cylindrically spreading waves (at frequencies of ω_1 and ω_2) confined between the planes $z = \pm l$ and within the half-planes including the z-axis and making angles $\pm\psi_1$ with the x-axis. It is further assumed that the radial power flow is uniformly distributed over the spreading angle of $2\psi_1$. In a practical case, this could be approximated to by assuming $2\psi_1$ to be the 3 dB beam width of the fan beam. Figure 7 indicates the geometry.

As cylindrical symmetry is assumed to exist within the fan beam, the pressure amplitude is uniform over the cylindrical surface defined by a = constant, bounded as detailed in the previous paragraph. If the amplitude of the differential pressure on such a surface due to a sinusoidal wave were P_a, then the power flow across the surface would be

$$W_a = \frac{P_a^2}{2\rho_0 c_0}(2la.2\psi_1). \tag{II.1}$$

The power flow W_a is independent of the radius a except for losses due to absorption)

Thus, if α is the absorption coefficient, $W_a \exp(2\alpha a)$ is independent of a and gives the transmitted acoustic power.

If the transmitted powers for the two primary waves in the fan beam are W_1 and W_2, then the instantaneous values of the differential pressure at a point at radius a due to the two waves are, respectively,

$$p_1 = (P_1/\sqrt{a}) \exp(-\alpha_1 a) \cos(\omega_1 t - k_1 a),$$
$$p_2 = (P_2/\sqrt{a}) \exp(-\alpha_2 a) \cos(\omega_2 t - k_2 a), \tag{II.2}$$

where α_1 and α_2, k_1 and k_2 represent the absorption coefficients and the wave-numbers at the frequencies ω_1 and ω_2, respectively, and

$$P_1 = [\rho_0 c_0 W_1/2l\psi_1)]^{1/2}.$$
$$P_2 = [\rho_0 c_0 W_2/(2l\psi_1]^{1/2}. \tag{II.3}$$

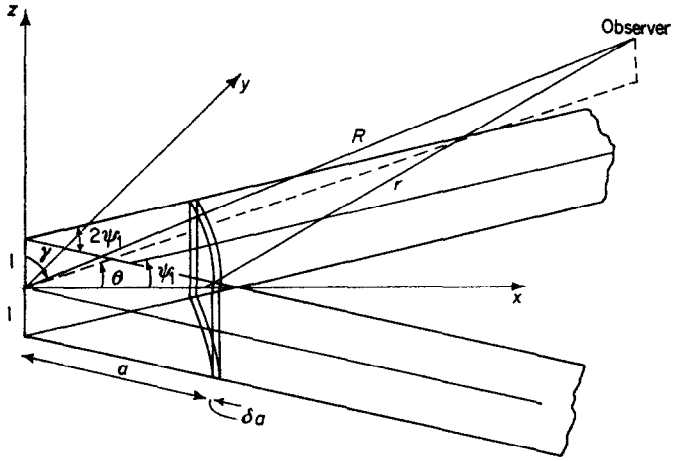

Figure 7. The geometry used. End-fire array formed by cylindrically spreading primary waves.

Substitution into the Westervelt source density expression for the difference frequency gives

$$q = -\frac{P_1 P_2}{\rho_0^2 c_0^4 a} \exp(-\overline{\alpha_1 + \alpha_2}\, a) \sin(\Omega t - Ka). \tag{II.4}$$

"Ω" is the difference frequency and "K" the associated wave-number. [It has been pointed out by V. G. Welsby (unpublished memorandum) and Smith (6) that Westervelt's expression for the source density is strictly applicable only for the interaction between plane waves. However, the expression is valid provided the acoustic impedance of the medium to the primary waves at the point of interaction is approximately equal to $\rho_0 c_0$, the plane wave impedance. At the frequencies of interest, this approximation can be justified and thus the source density expression may be used without modification for spherically or cylindrically spreading waves.]

Calculating the differential pressure at the difference frequency at a point (R, γ, θ) in the far field, due to the source contained in an elemental volume and of density q, and integrating successively over (i) z, between the limits $-l$ and $+l$, and (ii) a, between the limits 0 and ∞, gives

$$\mathrm{d}p = \frac{P_1 P_2 \Omega^2}{\rho_0 c_0^4 4\pi R} \exp(-\alpha R) \frac{2 \sin(Kl \cos\gamma)}{k \cos\gamma} \times$$
$$\times \frac{A \cos(\Omega t - KR) + K(1 - \sin\gamma \cos\overline{\theta - \psi}) \sin(\Omega t - KR)}{A^2 + K^2(1 - \sin\gamma \cos\theta - \psi)^2} \mathrm{d}\psi, \tag{II.5}$$

where $A \equiv \alpha_1+\alpha_2-\alpha\sin\gamma\cos\overline{\theta-\psi}$ and α is the absorption coefficient at the difference frequency.

Integration of this expression over ψ between the limits $-\psi_1$ and $+\psi_1$ would give the pressure distribution in the far field.

PRESSURE DISTRIBUTION IN THE FAR FIELD IN THE xy-PLANE

For a point on the xy-plane, $\gamma = \pi/2$. Thus, in (II.5),

$$\frac{2\sin(Kl\cos\gamma)}{K\cos\gamma} = 2l. \tag{II.6}$$

Also,

$$\begin{aligned} A &= \alpha_1+\alpha_2-\alpha\cos(\theta-\psi) \\ &\doteqdot \alpha_1+\alpha_2-\alpha, \end{aligned} \tag{II.7}$$

if $|\theta-\psi|$ is small and, further, the difference frequency is small compared with ω_1 and ω_2. Then,

$$p(R,\theta) = \frac{P_1P_2\Omega^2}{4\pi R}2l\exp(-\alpha R)\left\{\int_{\psi=-\psi_1}^{\psi_1}\frac{A\cos(\Omega t-KR)\,d\psi}{A^2+[2K\sin^2(\overline{\theta-\psi}/2)]^2}\right.$$

$$\left.+\int_{\psi=-\psi_1}^{\psi_1}\frac{2K\sin^2(\overline{\theta-\psi}/2)\sin(\Omega t-KR)}{A^2+[2K\sin^2(\overline{\theta-\psi}/2)]^2}\,d\psi\right\}. \tag{II.8}$$

If attention is restricted to small values of ψ_1 and θ such that $|\theta-\psi_1| \ll 1$, and hence

$$\sin^2(\overline{\theta-\psi}/2) \doteqdot (\overline{\theta-\psi}/2)^2, \tag{II.9}$$

then the integrals of equation (II.8) can be evaluated in a closed form.

The integrals in (II.8) reduce, respectively, to

$$I_1 = \int_{\psi=-\psi_1}^{\psi_1}\frac{A\,d\psi}{A^2+[2K\sin^2(\theta-\psi/2)]^2} \doteqdot \sqrt{2/(KA)}\int_{u=u_2}^{u_1}\frac{du}{1+u^4}, \tag{II.10}$$

and

$$I_2 = \int_{\psi=-\psi_1}^{\psi_2}\frac{2K\sin^2(\overline{\theta-\psi}/2)\,d\psi}{A^2+[2K\sin^2(\overline{\theta-\psi}/2)]^2} \doteqdot \sqrt{2/(KA)}\int_{u=u_1}^{u_1}\frac{u^2\,du}{1+u^4}, \tag{II.11}$$

when the inequality (II.9) holds. Here,

$$\begin{aligned} u &= \theta_0-\psi_0, \\ u_1 &= \theta_0-\psi_d, \\ u_2 &= \theta_0-\psi_d, \\ \theta_0 &= \theta/\theta_d, \\ \psi_0 &= \psi/\theta_d, \\ \psi_d &= \psi_1/\theta_d, \\ \theta_d &= \sqrt{(2A/K)}. \end{aligned} \tag{II.12}$$

Integrating through, one obtains

$$\begin{aligned} I_1 &= (1/4)(KA)^{-1/2}(\Phi+L), \\ I_2 &= (1/4)(KA)^{-1/2}(\Phi-L), \end{aligned} \tag{II.13}$$

where

$$\exp(L) = \frac{[(\theta_0^2-\psi_d^2)-\sqrt{2}\,\psi_d]^2+(1+\sqrt{2}\,\psi_d)^2}{[\theta_0^2-\psi_d^2+\sqrt{2}\,\psi_d]^2+(1-\sqrt{2}\,\psi_d)^2},$$

and

$$\Phi = -2\tan^{-1}(\sqrt{2}u_1+1)^{-1}+\tan^{-1}(\sqrt{2}u_1-1)^{-1}-\tan^{-1}(\sqrt{2}u_2+1)^{-1} - \tan^{-1}(\sqrt{2}u_2-1)^{-1}. \tag{II.14}$$

From equation (II.8), the amplitude of the differential pressure at a point (R,θ) in the xy-plane is given by

$$P(R,\theta) = \frac{P_1 P_2 \Omega^2}{4\pi R} 2l \exp(-\alpha R)(I_1^2+I_2^2)^{1/2},$$

where I_1 and I_2 are the integrals of (II.10) and (II.11), respectively. Using equations (II.13),

$$P(R,\theta) = \frac{P_1 P_2 (2l)\Omega^2 \exp(-\alpha R)}{\rho_0 c_0^4 8\pi R\sqrt{2KA}}\sqrt{(\Phi^2+L^2)}, \tag{II.15}$$

where Φ and L have the values given in (II.14).

It is worth noting that both Φ and L are functions of the normalized angular parameters ψ_d and θ_0, and independent of the distance variable R, while the remainder of the expression for $P(R,\theta)$ is independent of the normalized angular variable θ_0 and depends upon R. Thus, for a given value of R, the directivity pattern of the fan shaped end-fire array of virtual sources is determined by the expression $\sqrt{(\Phi^2+L^2)}$.

Further, for given acoustic powers in the primary beams, P_1 and P_2 depend upon the primary beam angle $2\psi_1$. From equations (II.3) and (II.15), the differential pressure amplitude $P(R,\theta)$ may be written in the form

$$P(R,\theta) = \frac{\sqrt{W_1 W_2}\,\Omega^2}{16\pi c_0^3 RA}\exp(-\alpha R)\frac{1}{\psi_d}\sqrt{(\Phi^2+L^2)}. \tag{II.16}$$

Comparing this result with equation (I.9) of Appendix 1, one obtains

$$P(R,\theta) = [P(R,0)]_1 \frac{1}{8\psi_d}\sqrt{(\Phi^2+L^2)}, \tag{II.17}$$

where $[P(R,0)]_1$ indicates the expression for $P(R,0)$ given in equation (I.9).

Now, from equation (I.10), it transpires that the directivity function $D(\theta)$ of (I.10) can be replaced by the expression

$$D_c(\theta_o,\psi_d) = \frac{1}{8\psi_d}\sqrt{(\Phi^2+L^2)} \tag{II.18}$$

when the primary waves consist of fan beams of cylindrically spreading waves instead of collimated plane waves.

DIFFERENTIAL PRESSURE AMPLITUDE ALONG THE AXIS OF SYMMETRY OF THE PRIMARY BEAMS

Along the axis of symmetry, $\theta = \theta_0 = 0$. Thus, from (II.14),

$$\Phi = -4[\tan^{-1}(\sqrt{2}\psi_d+1)^{-1}+\tan^{-1}(\sqrt{2}\psi_d-1)],$$

$$\exp(L/2) = \frac{\psi_d^2+\sqrt{2}\psi_d+1}{\psi_d^2-\sqrt{2}\psi_d+1}. \tag{II.19}$$

By using the values for L and Φ obtained from (II.19) in the equation (II.18), $D_0(o,\psi_d)$ was computed for various values of ψ_d. The results are plotted in Figure 8. These results show that provided half the fan beam angle, ψ_1, is not much larger than θ_d as given in

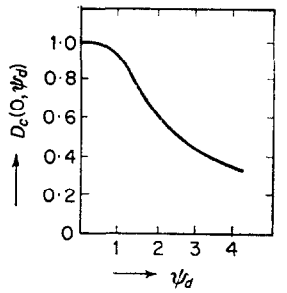

Figure 8. Difference frequency pressure amplitude along the axis as a function of primary beam width in units of $2\theta_d$ (Cylindrical primary waves).

equation (I.12), the scattered pressure amplitude along the axis of symmetry in the case studied in this Appendix is of the same order of magnitude as the corresponding quantity in the case studied in Appendix I. In fact, when $\psi_d \gg 1$ the two quantities are expected to be approximately equal.

BEAM WIDTH AT THE DIFFERENCE FREQUENCY

The directivity function $D_c(\theta_o,\psi_d)$ was calculated for various values of ψ_d, varying θ_o over a wide range for each value of ψ_d. Thus, a series of directionality patterns was obtained for the scattered field at the difference frequency, each curve being for a selected value of

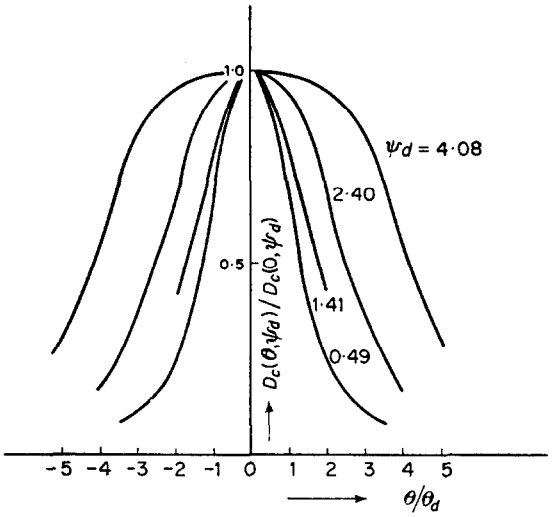

Figure 9. Interaction between cylindrically spreading primary beams: some directivity patterns of difference frequency waves.

ψ_d. These are shown in Figure 9. From these patterns, the 3 dB beam widths were calculated for various values of ψ_d, these values are shown plotted in Figure 10, both axes being in units of θ_d. Thus, as in the previous paragraph, one can conclude that provided ψ_d is not large, no appreciable deterioration occurs in the beam width at the difference frequency if the primary waves are cylindrical rather than plane.

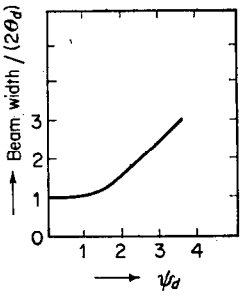

Figure 10. Beam width of difference frequency waves as a function of primary beam width. (Cylindrical primary waves.)

APPENDIX 3

SPHERICALLY SPREADING WAVES

In this Appendix the primary waves are assumed to be confined within a conical "pencil beam" of width $2\psi_1$; further, the intensity is assumed to be independent of the angular position of the observer at all points within this cone.

As the solid angle at the apex of the cone is $2\pi(1-\cos\psi_1)$, then, for a sinusoidal wave, the intensity at a point of distance a from the apex is

$$P^2/(2\rho_0 c_0) = W\exp(-2\alpha a)[2\pi a^2(1-\cos\psi_1)]^{-1}, \tag{III.1}$$

where W is the transmitted power and P is the amplitude of the differential pressure at a.

Therefore, the instantaneous values of the differential pressure at a point at a radius a due to the two primary waves are

$$\left.\begin{aligned} p_1 &= (P_1/a)\exp(-\alpha_1 a)\cos(\omega_1 t - k_1 a) \\ p_2 &= (P_2/a)\exp(-\alpha_2 a)\cos(\omega_2 t - k_2 a) \end{aligned}\right\}, \tag{III.2}$$

where

$$P_{1,2} = \sqrt{\rho_0 c_0 W_{1,2}}[\pi(1-\cos\psi_1)]^{-1/2}. \tag{III.3}$$

Following a similar procedure to that used in Appendix 2, one obtains for the differential pressure at the difference frequency at a point (R,θ) in the far field

$$p(R,\theta) \doteq \frac{P_1 P_2 \Omega^2}{2\rho_0 c_0^4 R}\exp(-\alpha R)\int_{\psi=0}^{\psi_1}\int_{a=0}^{\infty}\exp(-Aa)\,J_0(ak\sin\theta\sin\psi) \times \sin\psi\cos[\Omega t - KR - Ka(1-\cos\theta\cos\psi)]\,d\psi\,da, \tag{III.4}$$

where $A = \alpha_1+\alpha_2-\alpha\cos\theta\cos\psi$, which reduces to

$$A \doteq \alpha_1+\alpha_2-\alpha, \tag{III.5}$$

especially for small values of θ and ψ [see comments following equation (II.7) in Appendix 2].

By substituting

$$\left.\begin{aligned} E &= K(1-\cos\theta\cos\psi) \\ F &= K\sin\theta\sin\psi \end{aligned}\right\}, \tag{III.6}$$

one obtains, for the double integral of (III.4),

$$\frac{1}{2}\int_{\psi=0}^{\psi_1}\left\{\frac{\exp[j(\Omega t-KR)]}{[(A-jE)^2+F^2]^{1/2}}+\frac{\exp[-j(\Omega t-KR)]}{[(A+jE)^2+F^2]^{1/2}}\right\}\sin\psi\,d\psi. \tag{III.7}$$

A general solution of this integral is rather cumbersome. The special case of $\theta = 0$, corresponding to the pressure field along the axis of symmetry of the transducer, is of interest and is considered below.

DIFFERENTIAL PRESSURE AT THE DIFFERENCE FREQUENCY AT A POINT ALONG THE AXIS OF SYMMETRY

When $\theta = 0$, equation (III.4) reduces to

$$p(R,0) \doteq \frac{P_1 P_2 \Omega^2}{2\rho_0 c_0^4 R} \exp(-\alpha R) \int_{\psi=0}^{\psi_1} \int_{a=0}^{\infty} \exp(-Aa) \cos[\Omega t - KR - Ka(1-\cos\psi)] \times \times \sin\psi \, d\psi \, da \tag{III.8}$$

Integration, first over a and then over $\cos\psi$, gives

$$p(R,0) = \frac{P_1 P_2 \Omega^2}{2\rho_0 c_0^4 RK} \exp(-\alpha R) \left\{ \tfrac{1}{2} \log_e \left[1 + \frac{K^2}{A^2} (1-\cos\psi_1)^2 \right] \sin(\Omega t - KR) + \tan^{-1}[(K/A)(1-\cos\psi_1)] \cos(\Omega t - KR) \right\}, \tag{III.9}$$

in which use has been made of the definitions provided in equation (II.12) of Appendix 2. For small values of ψ_1 such that $(1-\cos\psi_1) \doteq \psi_1^2/2$,

$$(K^2/A^2)(1-\cos\psi_1)^2 \doteq (\psi_1/\theta_d)^4 \doteq \psi_d^4. \tag{III.10}$$

Thus, equation (III.8) becomes

$$p(R,0) \doteq \frac{P_1 P_2 \Omega^2}{2\rho_0 c_0^4 RK} \exp(-\alpha R) \{ \tfrac{1}{2} \log_e (1+\psi_d^4) \sin(\Omega t - KR) + \tan^{-1}(\psi_d^2) \cos(\Omega t - KR) \}. \tag{III.11}$$

The pressure amplitude is then given by

$$P(R,0) = \frac{P_1 P_2 \Omega^2}{2\rho_0 c_0^4 RK} \exp(-\alpha R) \{ [\tfrac{1}{2} \log_e (1+\psi_d^4)]^2 + [\tan^{-1}(\psi_d^2)]^2 \}^{1/2}. \tag{III.12}$$

Substituting for P_1 and P_2 from (III.3), one obtains

$$P(R,0) = \frac{\sqrt{W_1 W_2}\, \Omega^2}{2\pi c_0^3 RA} \exp(-\alpha R) \frac{1}{\psi_d^2} \{ [\tfrac{1}{2} \log_e (1+\psi_d^4)]^2 + [\tan^{-1}(\psi_d^2)]^2 \}^{1/2}. \tag{III.13}$$

Comparing this result with those of (I.9) of Appendix 1 and (II.17) and (II.18) of Appendix 2, one can write

$$P(R,0) = [P(R,0)]_1 D_s(0,\psi_d) \tag{III.14}$$

where $[P(R,0)]_1$, is the axial pressure amplitude when the primary waves are plane and

$$D_s(0,\psi_d) = \frac{1}{\psi_d^2} \{ [\tfrac{1}{2} \log_e (1+\psi_d^4)]^2 + [\tan^{-1}(\psi_d^2)]^2 \}^{1/2}. \tag{III.15}$$

$D_s(0,\psi_d)$ was computed for various values of ψ_d. The results, which are plotted in Figure 11, show that provided the pencil beam angle $2\psi_1$ is of the order of $2\theta_d$, as defined in Appendix 1, the amplitude of the differential pressure along the axis of symmetry would be expected to be of the same order in the case of spherically spreading waves as for plane primary waves.

Because a general solution was not found to the integral (III.7), no general conclusion can be reached about the directivity pattern at the difference frequency. However, it would seem to be fair to conclude that the beam width is of the order of $2\theta_d$, provided

that the amplitude of the differential pressure along the axis does not fall off; i.e., provided that ψ_d is not much greater than unity. The discussion at the end of Appendix 2 would appear to support this conclusion.

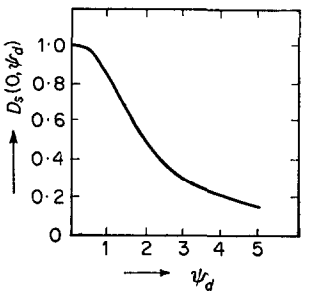

Figure 11. Variation of axial pressure at difference frequency with beam width of primary waves when the latter are spreading spherically.

APPENDIX 4

NON-LINEAR EFFECTS ASSOCIATED WITH THE PROPAGATION OF A PULSED CARRIER

In the case to be considered in this Appendix the primary wave is assumed to be plane and collimated, the pressure referred back to $x = 0$ being

$$p_i(t) = P_1 f(t) \cos \omega_1 t, \tag{IV.1}$$

where $f(t)$ is an envelope function which is assumed to vary slowly compared with the $\cos \omega_1 t$ term, and to have a maximum value of unity. The results in Appendices 2 and 3 show that even if the primary wave(s) are spreading cylindrically or spherically, this approach is valid provided the beam width is not too large compared with $2\theta_d$, as given by equation (I.12).

The pressure wave travelling into the medium is attenuated, the attenuation constant being, in general, a function of frequency. However, as the envelope function $f(t)$ is assumed to cover a relatively small frequency band, the attenuation constant for all the frequency components can be taken to be α_1 (i.e., that at the carrier frequency ω_1).

Hence

$$p_i(t, x) = P_1 \exp(-\alpha_1 x) f\left(t - \frac{x}{c_0}\right) \cos(\omega_1 t - k_1 x), \tag{IV.2}$$

giving

$$p_i^2(t, x) = (1/2) P_1^2 \exp(-2\alpha_1 x) f^2\left(t - \frac{x}{c_0}\right) [1 + \cos(2\omega_1 t - 2k_1 x)]. \tag{IV.3}$$

If the carrier frequency is sufficiently high, both the original signal and the $2\omega_1$ term arising from equation (IV.3) are attenuated relatively rapidly. The non-sinusoidal term of equation (IV.3) gives rise to a pressure component which is to be investigated in further detail. Substitution of this component of p_i^2 into the expression for the source density function gives

$$q = \frac{P_1^2}{2\rho_0^2 c_0^4} \exp(-2\alpha_1 x) \frac{\partial}{\partial t} \left\{ f^2\left(t - \frac{x}{c_0}\right) \right\}. \tag{IV.4}$$

In this case the source density component is not a single frequency one but covers a band of frequencies. Therefore, to calculate the radiated field it is more expedient to use frequency-space analysis.

The following Fourier pairs are used: $f(t)\leftrightarrow F(j\omega)$; $f^2(t)\leftrightarrow F_0(j\omega)$; $q(t)\leftrightarrow Q(j\omega)$; $\phi(t)\leftrightarrow\Phi(j\omega)$; $p(t)\leftrightarrow P(j\omega)$. (IV.5)

Thus,

$$Q(j\omega)\exp(-j\omega x/c_0) = \frac{P_1^2}{2\rho_0^2 c_0^4}\exp(-2\alpha_1 x)j\omega F_0(j\omega)\exp(-j\omega x/c_0). \quad \text{(IV.6)}$$

By using the approach indicated in Appendix 1, the Fourier Transform of the velocity potential at a point (R, θ) in the far field can be calculated as

$$\Phi(j\omega, R, \theta) = \frac{SQ(j\omega)}{4\pi R}\exp\left[-\left(\alpha + i\frac{\omega}{c_0}\right)R\right]\int_{x=0}^{\infty}\exp\left[-\left(2\alpha_1+\alpha+j\frac{\omega}{c_0}\overline{1-\cos\theta}\right)x\right]dx, \quad \text{(IV.7)}$$

where S is the cross-sectional area of the primary column, the dimensions of which are considered to be small compared with the wavelength at the frequencies of interest. At these frequencies, the absorption coefficient is also likely to be negligible. Further, since

$$p(t, R, \theta) = -\rho_0\frac{\partial}{\partial t}\{\phi(t, R, \theta)\},$$

[i.e., $P(j\omega) = -j\omega\rho_0\Phi(j\omega)$ at the point (R, θ)], then (IV.7) gives

$$P(j\omega) = \frac{P_1^2 S}{8\pi\rho_0 c_0^4 R\alpha_1}\frac{\omega^2 F_0(j\omega)\exp(-j\omega R/c_0)}{1+j\omega\sin^2(\theta/2)/(\alpha_1 c_0)}. \quad \text{(IV.8)}$$

In a later part of this Appendix it is shown that the energy contained within the pressure pulse [which is the inverse transform of the expression in (IV.8)] is concentrated in a rather narrow beam, corresponding to small values of θ. For a point along the axis of symmetry of the transducer (i.e., for $\theta = 0$),

$$p(t) = \frac{P_1^2 S}{8\pi\rho_0 c_0^4 R\alpha_1}\frac{\partial^2}{\partial t^2}\left\{f^2\left(t-\frac{R}{c_0}\right)\right\}. \quad \text{(IV.9)}$$

CONSIDERATIONS REGARDING THE PEAK TRANSMITTED POWER AND PULSE ENERGY

As the envelope function $f(t)$ has a maximum value of unity, the peak transmitted power, W_0 is given by

$$W_0 = \frac{P_1^2 S}{2\rho_0 c_0}, \quad \text{(IV.10)}$$

while the energy of the transmitted wave is

$$E_0 = W_0\int_{t=-\infty}^{\infty} f^2(t)\,dt \quad \text{(IV.11)}$$

or

$$E_0 = \frac{W_0}{2\pi}\int_{w=-\infty}^{\infty}|F(j\omega)|^2\,d\omega.$$

CONSIDERATIONS REGARDING THE PULSE ENERGY AT POINT (R, θ)

The energy in the pulse at the point (R, θ) is

$$E = \frac{1}{2\pi\rho_0 c_0}\int_{w=-\infty}^{\infty}|P(j\omega, R, \theta)|^2\,d\omega. \quad \text{(IV.12)}$$

From (IV.8), (IV.10) and (IV.12),

$$E = \frac{W_0^2}{32\pi^3 \rho_0 c_0^7 R^2 \alpha_1^2} \int_{w=-\infty}^{\infty} \frac{\omega^4 |F_0(j\omega)|^2}{1+\omega^2 V^2} \, d\omega, \tag{IV.13}$$

where

$$V = \frac{\sin^2(\theta/2)}{\alpha_1 c_0}.$$

Alternatively, from (IV.11) and (IV.13),

$$E/E_0 = \frac{\int_{w=-\infty}^{\infty} \frac{\omega^4 |F_0(j\omega)|^2}{1+\omega^2 V^2} . d\omega}{\left[\int_{t=-\infty}^{\infty} f^2(t)\, dt\right]^2} \frac{E_0}{32\pi^3 \rho_0 c_0^7 R^2 \alpha_1^2}. \tag{IV.14}$$

EXAMPLE: GAUSSIAN ENVELOPE FUNCTION

Let

$$f(t) = \exp(-n^2 t^2). \tag{IV.15}$$

Then

$$F(j\omega) = \frac{\sqrt{\pi}}{n} \exp\left(-\frac{\omega^2}{4n^2}\right).$$

Also,

$$F_0(j\omega) = \frac{\sqrt{(\pi/2)}}{n} \exp\left(-\frac{\omega^2}{8n^2}\right) \tag{IV.16}$$

as

$$f^2(t) = \exp(-2n^2 t^2).$$

The energy in the transmitted pulse is then

$$E_0 = \frac{\sqrt{(\pi/2)}}{n} W_0. \tag{IV.17}$$

THE ENERGY IN THE PULSE AT A POINT (R, θ) AND THE DIRECTIONALITY OF THE PRESSURE WAVE

From (IV.13) and (IV.16),

$$E(R,\theta) = \frac{W_0^2}{32\pi\rho_0 c_0^7 R^2 \alpha_1^2} \frac{1}{2\pi n^2} \int_{w=-\infty}^{\infty} \frac{\omega^4 \exp\left(-\frac{\omega^2}{4n^2}\right)}{1+\omega^2 V^2} d\omega. \tag{IV.18}$$

The general solution for the integral

$$I = \frac{1}{2\pi n^2} \int_{w=-\infty}^{\infty} \frac{\omega^4 \exp\left(-\frac{\omega^2}{4n^2}\right)}{1+\omega^2 V^2} d\omega \tag{IV.19}$$

can be obtained in the form

$$I = \frac{(2n)^3}{\sqrt{\pi}} [N - 2N^2 + 2\sqrt{\pi} N^{5/2} \exp(N)(1 - \operatorname{erf}\sqrt{N})], \tag{IV.20}$$

where

$$\sqrt{N} = \frac{1}{2n} \frac{\alpha_1 c_0}{\sin^2(\theta/2)}$$

and

$$\operatorname{erf}\sqrt{N} = (2/\sqrt{\pi}) \int_{y=0}^{\sqrt{N}} \exp(-y^2)\,dy.$$

Part of the integral (IV.19) was evaluated by J. M. Layton; his results form the basis for equation (IV.20).

For $\theta = 0$, $\sqrt{N} \to \infty$. For large values of $\sqrt{N}$, however,

$$\exp(N)(1-\operatorname{erf}\sqrt{N}) = (\pi N)^{-1/2}\left[1-\frac{1}{2N}+\frac{1.3}{(2N)^2}-\ldots\right]. \tag{IV.21}$$

Thus, as $\theta \to 0$,

$$I \to \frac{3}{2\pi^{1/2}}(2n)^3\left[1-\frac{5}{2N}+\frac{5.7}{(2N)^2}-\ldots\right]. \tag{IV.22}$$

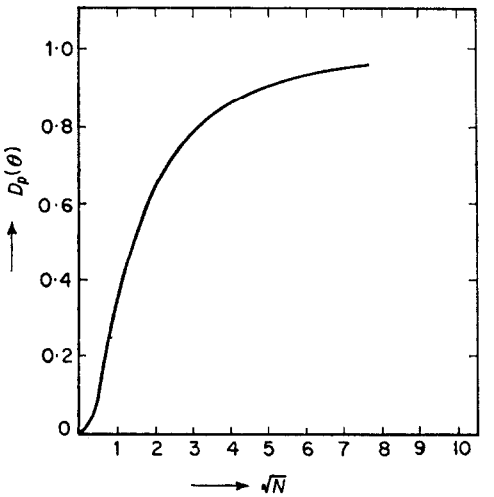

Figure 12. The directivity of pulse obtained from the self-modulation of a pulse carrier with a Gaussian envelope function.

As the expression for $E(R,\theta)$ is free from θ except through the parameter N, the ratio $D_p(\theta) = E(R,\theta)/E(R,0)$, giving the directivity of the pulse signal, can be formed by comparing the value of I from (IV.20) with that of $\operatorname{Lim}_{N\to\infty} I$ from (IV.22), i.e.,

$$D_p(\theta) = \tfrac{2}{3}[N - 2N^2 + 2\sqrt{\pi}N^{5/2}\exp(N)(1-\operatorname{erf}\sqrt{N})]. \tag{IV.23}$$

Thus, for large values of $\sqrt{N}$,

$$D_p(\theta) = 1-\frac{5}{2N}+\frac{5.7}{(2N)^2}-\frac{5.7.9}{(2N)^3}+\ldots. \tag{IV.24}$$

Values of $D_p(\theta)$ were computed for various values of $\sqrt{N}$ by using the expressions given in (IV.23) and in (IV.24). The results are shown plotted in Figure 12.

The 1/2 power point [i.e., the point at which $D_p(\theta) = 0.5$] is seen to correspond to $\sqrt{N} = 1.4$. Indicating the corresponding value of θ by θ_1 and considering only the positive root, one obtains

$$\sin(\theta_1/2) = \left[\frac{\alpha_1 c_0}{2.8n}\right]^{1/2}. \tag{IV.25}$$

The duration of the envelope pulse, $f(t)$, between its 1/e points is $T = 2/n$. Substituting for n in (IV.25) gives

$$\sin(\theta_1/2) = 0{\cdot}422\sqrt{(\alpha_1 c_0 T)}. \tag{IV.26}$$

In water, $c_0 \fallingdotseq 1{\cdot}5 \times 10^3$ msec and $\alpha_1 \ll 1$ provided that the carrier frequency is not in the region of many Mc/s ($\alpha_1 = 0{\cdot}04$ neper/m at 1 Mc/s).

Therefore, if the pulse duration, T, is of the order of a msec the magnitude of the right hand side of (IV.26) is much less than 1. Therefore,

$$\theta_1 \fallingdotseq 0{\cdot}844\sqrt{(\alpha_1 c_0 T)} \text{ radians.}$$

The beam width, $2\theta_1$, then is

$$2\theta_1 = 96{\cdot}5\sqrt{(\alpha_1 c_0 T)} \text{ degrees.}$$

TABLE 1

Beam width, $2\theta_1$, for various carrier frequencies and pulse durations

Carrier freq. (kc/s)	α_1†		$2\theta_1/\sqrt{t_m}$‡		Beam width, $2\theta_1$ $t_m = 1$ msec		$t_m = 0{\cdot}1$ msec	
	Fresh water	Sea water	Fresh water	Sea water	Fresh water	Sea water	Fresh water	Sea water
100	$3{\cdot}8 \times 10^{-4}$	$3{\cdot}3 \times 10^{-3}$	2·3	6·8	2·3	6·8	0·73	2·2
300	$3{\cdot}4 \times 10^{-3}$	8×10^{-3}	6·9	10·6	6·9	10·6	2·2	3·4
1000	$3{\cdot}8 \times 10^{-2}$	$4{\cdot}3 \times 10^{-2}$	23	24·5	23·0	24·5	7·3	7·8

† α_1 in nepers/m.
‡ θ_1 in degrees and t_m in msec.

Substituting $t_m = T \times 10^3$ and the value of c_0 for water, one finds

$$2\theta_1 = 118\sqrt{(\alpha_1 t_m)} \text{ degrees,} \tag{IV.27}$$

that is,

$$2\theta_1 t_m^{-1/2} = 118\sqrt{\alpha_1}, \tag{IV.28}$$

where t_m is a measure of the pulse length in msec and θ_1 is in degrees.

Table 1 was prepared from equation (IV.28) to show the values of $2\theta_1 t_m^{-1/2}$ for various carrier frequencies.

ENERGY IN THE PULSE ALONG THE AXIS OF THE TRANSDUCER

The equations (IV.18), (IV.19) and (IV.22) give, for the case of $\theta = 0$,

$$E(R,0) = \frac{3W_0^2 n^2}{8\pi^{3/2}\rho_0 c_0^7 \alpha_1^2 R^2}. \tag{IV.29}$$

From (IV.17) and (IV.29) one can obtain

$$E_{eq}/E_0 = 4\pi R^2 E(R,0)/E_0 = \frac{3n^5 E_0}{\pi^{3/2}\rho_0 c_0^7 \alpha_1^2} \tag{IV.30}$$

The left-hand side of equation (IV.30) represents the ratio of E_{eq}, the omnidirectional energy required to produce the pulse energy $E(R,0)$, to the transmitted energy E_0.

For water this is

$$E_{eq}/E_0 = \frac{E_0}{t_m^5 \alpha_1^2} \times 10^{-9}. \tag{IV.31}$$

For fresh water, at a carrier frequency of 100 kc/s, $\alpha_1 = 4 \times 10^{-4} N/m$. Then the right hand side of (IV.31) becomes $6{\cdot}25 \times 10^{-3} E_0 t_m^{-5}$. For a pulse duration of the order of 0·1 msec, this is $625\, E_0$.

APPENDIX 5

SYMBOLS

P, p†	pressure, as defined in the text
p_i	total differential pressure at a point due to the primary waves
ρ_0	density of the undisturbed medium
c_0	velocity of propagation of sound in an undisturbed medium
α†	absorption coefficient of the medium
A	an absorption function, as defined in test, normally of the value $\alpha_1 + \alpha_2 - \alpha$
ω_1, ω_2 or f_1, f_2	primary frequencies
k_1, k_2	wave-numbers at primary frequencies
Ω, K	difference frequency and the corresponding wave-number
q	source density
ϕ	velocity potential

† Normally, a subscript (1) or (2) is used to denote value pertaining to the primary frequencies, while the value at the difference frequency is indicated without a subscript.

REFERENCES

1. Lord Rayleigh 1877 *Theory of Sound* (two volumes). New York: Dover Publications, second edition, 1945 re-issue.
2. P. J. Westervelt 1957 *J. acoust. Soc. Am.* **29**, 199. Scattering of sound by sound.
3. M. J. Lighthill 1952 *Proc. R. Soc.* **A211**, 564. On sound generated aerodynamically.
4. J. L. S. Bellin and R. T. Beyer 1962 *J. acoust. Soc. Am.* **34**, 1051. Experimental investigation of an end-fine array.
5. H. O. Berktay and B. V. Smith 1965 *Electronics Letters* **1**, 6.
6. B. V. Smith 1964 *University of Birmingham Department of Electronic and Electrical Engineering Memorandum* 219.
7. P. J. Westervelt 1960 *J. acoust. Soc. Am.* **32**, 934A. Parametric end-fire array.
8. R. T. Beyer 1960 *J. acoust. Soc. Am.* **32**, 719. Parameters of non-linearity in fluids.
9. A. Freedman 1960 *J. acoust. Soc. Am.* **32**, 197. Sound field of a rectangular piston.
10. S. R. Murphy, G. R. Garrison and D. S. Potter 1958 *J. acoust. Soc. Am.* **30**, 871. Sound absorption at 50 to 500 kc from transmission measurements in the sea.
11. T. F. Hueter and R. H. Bolt 1955 *Sonics*. London: Chapman and Hall.
12. R. P. Barnes, Jr. and R. T. Beyer 1964 *J. acoust. Soc. Am.* **36**, 1371. Ultrasonic absorption in water at finite amplitudes.
13. H. Lamb 1931 *The Dynamical Theory of Sound*. New York: Dover Publications; second edition, 1960 re-issue.